Study on joint formation evolution in laser microwelding of Pt-10%Ir and 316 LVM SS crossed wires

Mao Jinrong[1, a], Huang Yongde[1, b *], and He Peng[2, c]

[1]School of Aeronautical Manufacturing Engineering, Nanchang Hangkong University, Nanchang, China, 330063
[2]School of Materials Science and Technology, Harbin Institute of Technology, Harbin, China, 150001

[a]maojinrong726@163.com, [b]huangydhm@nchu.edu.cn, [c]hepeng@hit.edu.cn

Keywords: Crossed wire, Laser microwelding, Simulation, Joint formation.

Abstract. In order to identify the evolution of joint formation about crossed wires of Pt-10% Ir to 316 LVM SS in laser microwelding, the experimental and computational study was carried out. The results showed that, with the increase of peak power of laser microwelding, the laser joint evolution of the crossed-wires appears a transition from a laser braze to a fusion weld. The simulation of joint was agreed with the experimental results.

Introduction

Special requirements of materials used in implantable medical devices include biocompatibility, corrosion resistance, and the capability of producing extremely high reliability joints [1]. Common materials that meet these requirements include 316 low-carbon vacuum melted (LVM) stainless steel (SS), titanium, niobium, NitinolTM, nickel-cobalt alloys such as MP35NTM and KovarTM, platinum, and platinum-iridium alloys [1]. The excellent mechanical properties and electrical conductivity of Pt alloys and 316 LVM SS make them ideal for biomedical applications including electrical terminals, wires, coils, and electrodes [2]. With the increasing complexity of medical devices and a constant drive for lower costs, the challenge of joining dissimilar biocompatible materials is presented. For example, the electrical terminals in pacemakers are made of a Pt-Ir alloy, while the interconnecting wires are made from SS. To reduce material costs, it is necessary to bond these dissimilar materials together.

Resistance microwelding (RMW) and laser micro- welding (LMW) are two of the most important joining processes applied to the small-scale fabrication of medical devices [1, 3, 4]. As acknowledged in recent publications, variations in resistivity hindered the application of RMW for dissimilar materials [5, 6]. Therefore, this results in a need to explore laser spot microwelding of dissimilar materials.

Current literature on microwelding of crossed wires focuses on RMW processes such as the joining of Ni sheets, bare and Au-plated Ni wires, 316 LVM SS, and 304 SUS SS [3, 4, 7, 8]. To date, only limited literature exists detailing the research on laser microwelding of crossed wire, this is especially true for dissimilar materials. Up to now, no report on laser spot microwelding of 316 LVM SS and Pt-Ir wires has been found. The objective of this study is to identify the crossed wire laser weldability of Pt-10% Ir wire to 316 LVM SS wire.

Experimental Procedure

Fully annealed 0.38 mm diameter Pt-10% Ir and cold-worked 316 LVM SS wires are bonded by laser spot microwelding in this study. The chemical composition of the 316 LVM SS wire is as follow: C, 0.024; Cr, 17.47; Ni, 14.73; Mo, 2.76; and others elements in Bal., in weight percent. Before welding, the wires are ultrasonically cleaned in acetone for 10 min to remove any surface contaminants. Welding is conducted using a Miyachi Unitek LW-50A Nd:YAG laser welding system, capable of 50 J pulsed energy and 5 kW peak power. The pulse profile used consists of a 0 ms

up-slope, 30 ms weld time followed by a 0 ms down-slope. The peak power is varied from 0.20 kW to 0.52 kW in this study.

Fig. 1 shows the schematic of the welding fixture used to position the wires 90° from one another. A small force is imposed by spring plates on the Pt wire located on the top to ensure intimate contact with the SS wire. A hole in the fixture located directly below the weld location prevents welding of the wires to the fixture. The hole has a depth (H) of 1mm and a diameter (φ) of 1 mm. Care was taken to ensure each weld is centred at the intercept of the two wires. A positioning laser is used to accurately determine the centre of the weld.

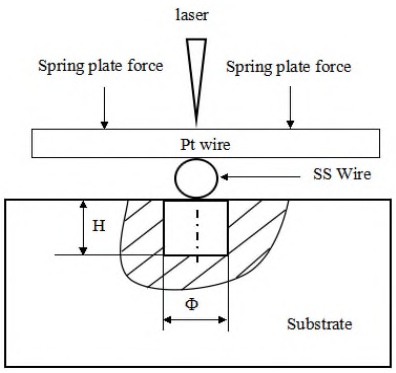

Fig. 1 Schematic of welding fixture.

A tensile testing in right angle is used to determine the joint breaking force (JBF). The tensile tests are performed using an Instron model 5548 microtensile tester manufactured by Instron, Massachusetts, USA at a crosshead speed of 4 mm/min. Three joints were tested for each set of welding conditions to obtain the average JBF. The surface appearance, fracture surfaces, and cross sections of the joints are examined using an energy dispersive X-ray spectroscopy (EDX) equipped scanning electron microscope (SEM).

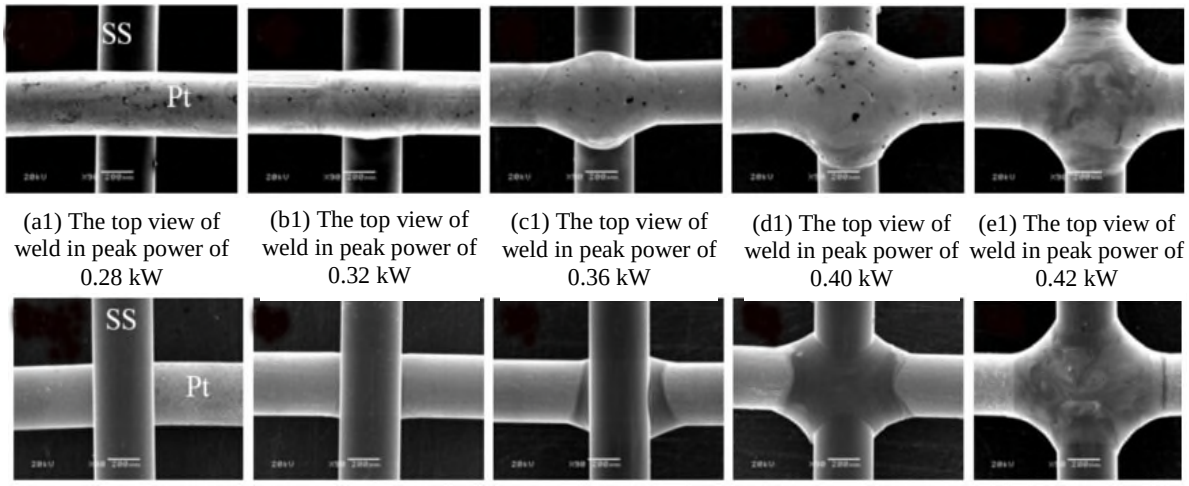

(a1) The top view of weld in peak power of 0.28 kW | (b1) The top view of weld in peak power of 0.32 kW | (c1) The top view of weld in peak power of 0.36 kW | (d1) The top view of weld in peak power of 0.40 kW | (e1) The top view of weld in peak power of 0.42 kW

(a2) The bottom view of weld in peak power of 0.28 kW | (b2) The bottom view of weld in peak power of 0.32 kW | (c2) The bottom view of weld in peak power of 0.36 kW | (d2) The bottom view of weld in peak power of 0.40 kW | (e2) The bottom view of weld in peak power of 0.42 kW

Fig. 2 Top and bottom surfaces of welded crossed wire joints.

Results

Welds Geometry. The top and bottom views of crossed wire welds produced using peak welding powers of 0.28 to 0.40 kW are shown in Fig. 2. At the lowest peak power of 0.28 kW little change is observed in either the top or bottom side of the joint [Fig. 2 (a1) and (a2)]. For peak powers of 0.32 kW to 0.40 kW, surface pores are observed on the top side of the joint (i.e. Pt-Ir wire side) that is subject to the incident laser beam [Fig. 2 (b1-d1) and (b2-d2)]. The number and size of the pores

increases with peak power. However, the surface porosity disappears with a peak power of 0.42 kW. No porosity is found on the bottom side (i.e. 316 LVM SS side) of the welds during this study. Increasing the peak power further causes the laser to drill through the weld which causes burn through type defects.

Joint Breaking Force (JBF). The effect of peak power on the JBF and fracture modes is shown in Fig. 3. At low peak powers from 0.26 kW to 0.32 kW the joint strength increases drastically. At a peak power of 0.32 kW, the JBF reaches 37.4 N which is 87 % of the 43 N tensile strength of the Pt-10% Ir wire. During the intermediate power range between 0.32 kW and 0.42 kW, the JBF decreases first then increases again at a peak power of 0.42 kW where the maximum JBF is achieved. The JBF decreases steadily for joints made with a peak power above 0.42 kW due to over-welding.

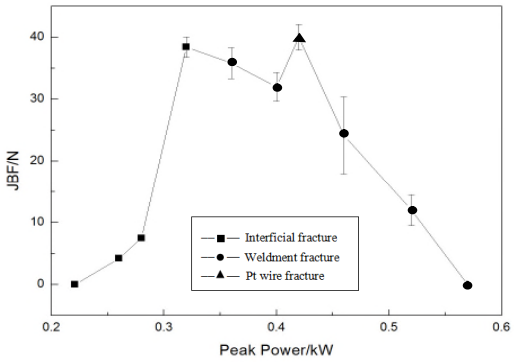

Fig. 3 Joint breaking force (JBF) measured during tensile testing.

Joint Cross Sections. Fig. 4 shows SEM micrographs obtained from cross section of joints made at various peak power. Fig. 5 shows high magnification images of initial joint.

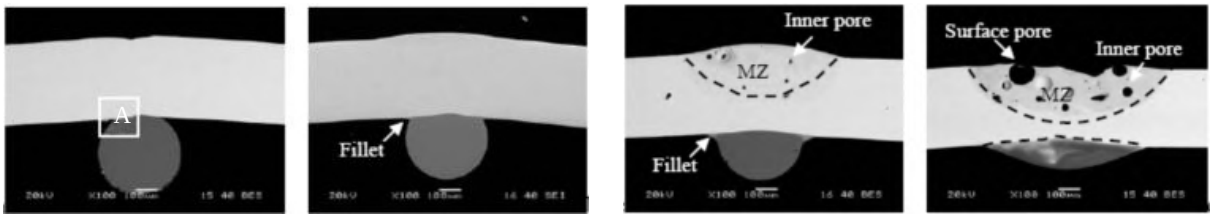

(a) 0.28 kW (b) 0.32 kW (c) 0.36 kW (d) 0.40 kW

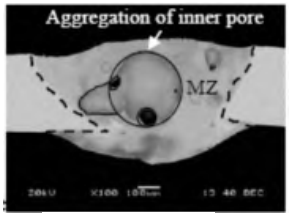

(e) 0.42 kW

Fig. 4 SEM images of joint cross sections along Pt-Ir wire axis with different peak powers.

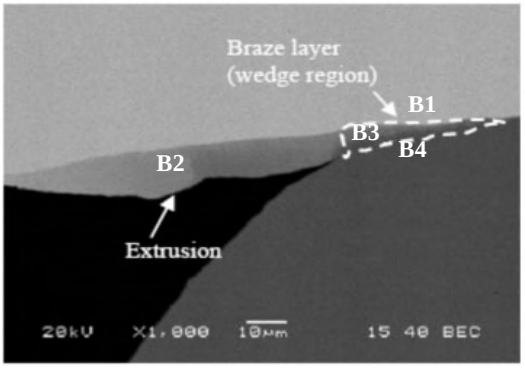

Fig. 5 High magnification SEM image of joint produced with a peak power of 0.28 kW from region A of Fig. 4(a).

There was no evident change at the interface of initial joint welded in peak power of 0.28kW (see Fig. 4a), but high magnification image detailed that the extrusion and braze layer formed in joint. Base on the EDX results (in Table 1), it can be confirmed that braze layer was formed in the wedge region of joint, which was resulted from no melting trace in adjacent regions of B1 and B4. The brazing layer (B3) and extrusion (B2) were Fe-Pt alloy with about 38% and 60% at pct. Pt content in fillet is higher than that in braze layer, which is due to longer reaction time for fillet with Pt wire. It can be seen that smooth fillet at the edge of the joint had been formed at peak power of 0.32kW and 0.36kW, as shown in Fig. 4b and 4c, which was same as the resistance microwelding of crossed Au-plated Ni wires. Increasing welding peak power resulted in more heat generation and hence more fillets produced. As a result, the Pt wires set down more into SS wires, leading to an increase in bond area. But, further increase of peak power, the mixture zone (MZ) could be clearly seen in the cross section. It is worth noting that the MZ should be found going through Pt wire, because the wholly penetration of Pt wire is necessary to form a joint, in facts, misalignment of cutting plate of cross separate from the SS wire.

The laser micro-welding of crossed 316LVM SS wire reported by I. Khan et al, revealed that fusion is the primary bonding mechanism. The present work shows that brazing and fusion bonding occurred during LMW of crossed 316LVM SS and Pt wire. In theory, fusion bonding should be the primary bonding mechanism if the crossed wires of similar material to be welded. Evidence of EDX analysis results of B in fracture surface (Fig. 4a) showed there was mixture of molten dissimilar in the center of weld. But in the rim of faying face from the SEM of joint interface, local braze bond was produced definitively, and also have strong bond strength, as a result of fracture of Pt wire in region A of Fig. 3a. The difference can be ascribed to the following aspects. In this case, SS has the lower melting point (1420 ºC) and heat conductive resistance, compared with Pt alloy, which makes SS wire easier to melt at interface. So the volume and area of melting of SS is larger than those of Pt, some of the molten SS metal distributed under the un-molten Pt wet Pt wire to form braze layer, the others was displaced from the interfacial zone to form the fillet, as shown in Fig. 4b and 4c. Therefore, as welding peak power increases, the bottom SS wire were molten entirely, leading to mixing with molten Pt and spread along the Pt wire, that is reason for no fillet formation in higher peak power.

Table 1. EDX analysis results of regions B1, B2, B3 and B4 from Fig. 5. All measurements are in atomic percent.

Position	Pt	Fe	Cr	Ni	Other elements
B1	74.47	1.63	-	4.30	10.09
B2	25.01	46.66	13.33	9.89	1.06
B3	11.96	51.49	14.19	15.16	4.59
B4	0.35	60.13	20.82	13.03	4.68

Simulations

An investigation regarding capability of MSC.Marc in simulation of welding is presented. The investigation focuses on temperature fields to identify the joint formation evolution [9].

Wires in diameter of 0.38mm made of 316 SS and Pt alloys were to be welded together. The highly hatched areas in Fig. 6 represent where the laser irradiated directly. 27200 units and 31395 node points were achieved. 2D Gaussian Heat Source Model as Eq. (1) was used. Process parameters are described in Table 2. Simulation using the assumed convective heat transfer boundary conditions was considered the radiation heat transfer by increasing the convective heat transfer coefficient properly. In addition, the latent heat of fusion was considered also.

To introduce the pulsed heat input in different peak power of laser irradiation, an in-house developed user subroutine is utilized. This allows the weld heat source to be simulated as an ellipsoidal heat source described by Goldak et al., [10].

Equation of heat source model is as follow:

$$q(r) = q_m \exp\left(-3\frac{r^2}{\bar{r}^2}\right) \tag{1}$$

q_m—heat flow at the center of pulse; $\bar{r}$ —effective distribution radius of heat source; r—distance away from the center of heat source.

Table 2. Physical properties of wires.

Property/IU	**316 LVM SS**	**Pt alloy**
Density/(kg/m^3)	8000	21500
Solidus temperature / ºC	1370	1790
Liquidus temperature / ºC	1410	1800
Solid thermal conductivity /(J/m·s·ºC)	16.3	31
Thermal diffusivity /(m^2/s)	10^{-6}	$2.4x10^{-5}$
Heat capacity(0-100 ºC) /(J/kg·ºC)	500	130
Latent heat of fusion (J/g)	247	101

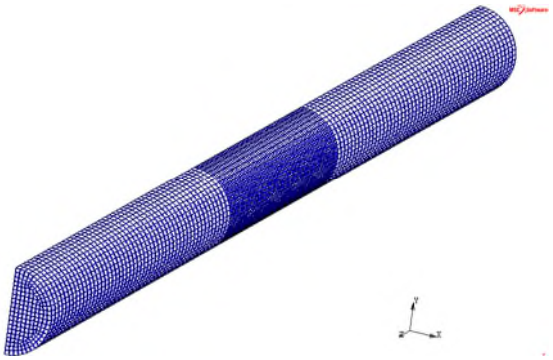

Fig. 6 Finite element mesh of wire.

The actual welding of the dissimilar wires takes 30 microseconds with different laser peak power. Fig. 7 shows the heat absorbed by the wire sat an arbitrarily chosen interval between t=0.6ms and t=30ms. Fig. 7 clearly shows a cyclic melting behavior of Pt alloy wire. The cycle spans 30 microseconds. In the center of the heat source, the temperature of bottom Pt alloy wire reaches 1400 ºC at approximately 17ms, which melts the SS wire downsides, contributes the brazing joint at interface. It is in accord with the observation in the experimental results.

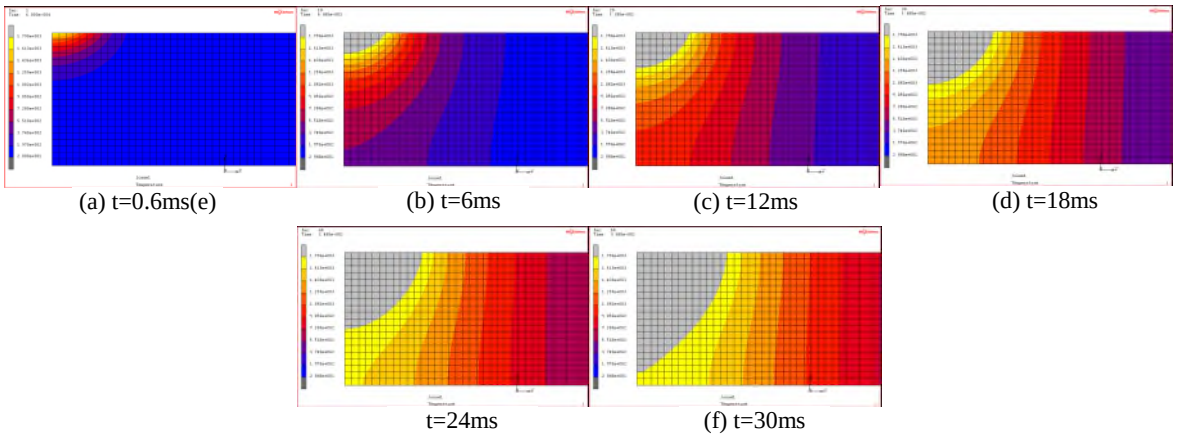

(a) t=0.6ms(e) (b) t=6ms (c) t=12ms (d) t=18ms

t=24ms (f) t=30ms

Fig. 7 Evolution of temperature fields in Pt alloy wire.

Conclusions

The weld geometry, the JBF and micrograph of LMW of crossed SS and Pt wires, as well as the simultion, have been investigated. The major conclusions are summarized as follows:

1) The laser joining evolution of the crossed-wires transitioned from a laser braze to a fusion weld with increasing peak power.

2) The optimum joint geometry and a JBF value was achieved with a peak power of 0.42 kW.

3) The simulation of cyclic melting behavior of Pt alloy wire further confirmed the joint formation evolution.

Acknowledgements

This work has been funded by Program of Canada Research Chairs (CRC) in Microjoining (www.crc.gc.ca) and National Natural Science Foundation of China (Grant No. 51365044). Thanks are due to Jianguo Yang for helping with the simulation of temperature field.

References

[1] Y. Norman Zhou, Microjoining and Nanojoining, Woodhead Publishing Ltd, Cambridge, 2008.

[2] N. J Noolu, H. W. Kerr, Y. Zhou, J. Xie, Laser weldability of Pt and Ti alloys, Mater. Sci. Eng. A. 397 (2005) 8–15.

[3] S. Fukumoto, Y. Zhou, Mechanism resistance microwelding of crossed fine nickel wires, Metallur. Mater. Trans. 35 (2004) 3165-3176.

[4] S. Fukumoto, Z. Chen, Y. Zhou, Interfacial phenomena and joint strength in resistance microwelding of crossed Au-plated Ni wires. Metallur. Mater. Trans. 36 (2005) 2717–2724.

[5] Z. Chen, Joint formation mechanism and strength in resistance microwelding of 316L stainless steel to Pt Wire, J. Mater. Sci. 42 (2007) 5756-5765.

[6] K. J. Ely, Y. Zhou, Microresistance spot welding of Kovar, steel, and nickel. Sci. Tech. Weld. Join. 6 (2001) 63–72.

[7] W. Tan, Y. Zhou, H. W. Kerr. Effects of Au plating on small-scale resistance spot welding of thin-sheet nickel. Metallur. Mater. Trans. A. 33 (2002) 2667-2676.

[8] M. I. Khan, J. M. Kim, M. L. Kuntz, Y. Zhou, Bonding mechanisms in resistance microwelding of 316 low-carbon vacuum melted stainless steel wires. Metallur. Mater. Trans. A, 40 (2009) 910-919.

[9] L. Tan, J. X. Zhang, D. Zhang, Prediction of welding residual stress in multi-pass narrow gap welded pipes with large thickness. China Welding. 23 (2014) 6-11.

[10] A. Goldak, M. Akhlaghi. Computational welding mechanics, Carleton University. New York, 2005.